Acta Pharmaceutica Sinica B 2018;8(4):587–601

Chinese Pharmaceutical Association
Institute of Materia Medica, Chinese Academy of Medical Sciences

Acta Pharmaceutica Sinica B

www.elsevier.com/locate/apsb
www.sciencedirect.com

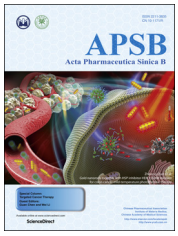

ORIGINAL ARTICLE

Gold nanorods together with HSP inhibitor-VER-155008 micelles for colon cancer mild-temperature photothermal therapy

Xichuan Tang[a,†], Liwei Tan[b,†], Kun Shi[a], Jinrong Peng[a], Yao Xiao[a], Wenting Li[c], Lijuan Chen[a], Qian Yang[d], Zhiyong Qian[a,*]

[a]*State Key Laboratory of Biotherapy, West China Hospital, West China Medical School, Sichuan University, and Collaborative Innovation Center, Chengdu 610041, China*
[b]*College of Medicine, Southwest Jiaotong University, Chengdu 610031, China*
[c]*Department of Pharmacy, West China Second University Hospital, Sichuan University, Chengdu 610041, China*
[d]*School of Pharmacy, Key College Laboratory of Sichuan Province for Specific Structure of Small Molecule Drugs, Chengdu Medical College, Chengdu 610500, China*

Received 30 March 2018; received in revised form 18 May 2018; accepted 18 May 2018

KEY WORDS

Tumor inhibitor;
VER-155008;
Micelle;
Phototherapy;
Gold nanorods

Abstract Enhancing the heat-sensitivity of tumor cells provides an alternative solution to maintaining the therapeutic outcome of photothermal therapy (PTT). In this study, we constructed a therapeutic system, which was composed of methoxy-polyethylene-glycol-coated-gold-nanorods (MPEG-AuNR) and VER-155008-micelles, to evaluate the effect of VER-155008 on the sensitivity of tumor cells to heat, and further investigate the therapeutic outcome of MPEG-AuNR mediated PTT combined with VER-155008- micelles. VER-155008- micelles down-regulate the expression of heat shock proteins and attenuate the heat-resistance of tumor cell. The survival of HCT116 cells treated with VER-155008- micelles under 45 °C is equal to that treated with high temperature hyperthermia (55 °C) *in vitro*. Furthermore, we proved either the MPEG-AuNR or VER-155008- micelles can be accumulate in the tumor site by photoacoustic imaging and fluorescent imaging. *In vivo* anti-cancer evaluation showed that tumor size remarkably decreased (smaller than 100 mm^3 or vanished) when treated with combing 45 °C mild PTT system, which contrasted to the tumor size when treated with individual 45 °C mild PTT (around 500 nm^3) or normal saline as control (larger than 2000 nm^3). These results proved that the VER-155008- micelles

*Correspondence address. Tel./fax: +86 28 85501986.
E-mail address: anderson-qian@163.com (Zhiyong Qian).
†These authors are the co-first authors for this work.
Peer review under responsibility of Institute of Materia Medica, Chinese Academy of Medical Sciences and Chinese Pharmaceutical Association.

https://doi.org/10.1016/j.apsb.2018.05.011

can attenuate the heat-resistance of tumor cells and enhance the therapeutic outcome of mild-temperature photothermal therapy.

1. Introduction

Although chemotherapy is one of the widely used clinical treatments for cancer[1] and hundreds of chemodrugs have been developed and applied in tumor therapy[2], the side-effects, auxiliary toxicity and the high risk excipients in traditional formulations limit the application of chemodrugs[3]. Finding an effective therapy with low side-effects deserves attention. The small-molecule inhibitors with low adverse reaction provide an alternative choice for cancer therapy, and the research and development of small-molecule inhibitors have been highlighted[4,5].

Small-molecule inhibitors inhibit tumors by inhibiting specific DNA, nucleic acid and proteins that relate to tumor growth and metastasis[6–8]. Unlike the non-targeting side-effects of chemodrugs, the small-molecule inhibitors specifically suppress the growth of the tumor cells with low adverse reaction[9]. Therefore, small-molecule inhibitors have attracted enormous attention in recent years[10–12]. VER-155008 is one of these potential small-molecule inhibitors, which can promote apoptosis to take place in the tumor cells by specifically reducing the expression of heat-shock proteins 70 and 90 (HSP70 and HSP90)[13–16]. As a member of the HSP family, HSP70 and HSP90 are involved in the folding and function of several proteins and essential for tumor cell survival by regulating the expression of oncogenic client proteins like RAS, p53 and AKT.[17] Besides, overexpression of HSP in the tumor site results in inefficiency of photothermal therapy (PTT) due to the tolerance of tumor cells to heat stress[18]. Therefore, reduction of HSP70 and HSP90 in tumor cells not only promotes the cells apoptosis, but also improves the heat-sensitivity of tumor cells[19–26]. Therefore, combining the PTT with VER might be a feasible way to enhance the anti-tumor effect[17]. However, the bioavailability of VER is also restricted by its hydrophobic character, similar to some other hydrophobic anti-tumor drugs[15,27].

Nano drug delivery systems have been applied to overcome the hydrophobicity of the cargo and enhance their delivery efficacy to the tumor site though the enhanced permeability and retention (EPR) effect[28–30]. More than 40 kinds of nano-formulations have been studied in clinical trials[31]. By being encapsulated into nanocarriers, the system improves the solubility of drugs, prevents renal clearance, promotes longer circulation in blood, responsiveness and enhances passive targeting to solid tumor sites[32–35]. Among numerous kinds of materials for nanocarrier construction, amphiphilic block copolymer methoxy polyethylene glycol-poly (D,L-lactic acid) (MPEG- PDLLA) has been approved by FDA in preparing the DTX micelle, which has been launched into the market in South Korea[36–41]. Bearing both hydrophobic and hydrophilic blocks within same polymer chain, amphiphilic copolymers can self-assemble and form different types of nanoparticular structures such as micelle[42]. Due to its superior drug loading ability and biocompatibility, we expected that MPEG-PDLLA could be used to load VER-155008 to form VER-155008 micelles (VER-M), therefore improving VER's water solubility and prolonging its blood circulation time. The introduction of VER-M may be more suitable for enhancing the therapeutic outcome of low temperature PTT (which is also called mild PTT)[43].

PTT is an efficient therapeutic process with low side-effects for cancer therapy[44,45]. Optically sensitive materials which exhibit efficient photothermal conversion can be used as PTT agents to generate heat under laser irradiation to ablate cancer[46,47]. Among different kinds of PTT agents, different types of gold nanoparticles (AuNPs) have long been a topic of intense research due to their size-related electronic, magnetic and optical properties[48], which was used for antibacterial, biosensing, imaging and cancer treatments[49]. Gold nanorod (AuNR) is one of the most effective agents in all these AuNPs for photothermal conversion[50–52]. By surface modification with MPEG-thiol (MPEG-SH, 5000 Da), more biocompatible AuNR (MPEG-AuNR) can be obtained[57] to overcome toxicity of AuNR[53]. Owing to the surface coating with MPEG and the EPR effect, MPEG-AuNR is more likely to accumulate in tumors[54]. Furthermore, AuNR can also be easily surface modified to functionalize[55,56]. MPEG-AuNR is a suitable agent for PTT.

According to the therapeutic temperature, PTT can be divided into hyperthermia ($>45\,^{\circ}C$) and mild PTT ($\leq 45\,^{\circ}C$)[58]. Although hyperthermia is usually more effective, adverse risks, including amatory disease and tumor metastasis, can happen. On the contrary, mild PTT has low side-effects but the ineffective therapeutic outcome as a result of high expression of HSPs remains a challenge[18]. Besides, improving the penetration depth of 700–950 nm NIR energy source to activate phototherapy is still desired, which lead to low temperature PTT[59]. Thus, it is imperative to attenuate heat-resistance in mild PTT by using an HSP inhibitor, and VER-M can be used as one of the potential high-performance HSP inhibitors[60].

Therefore, in this study, we plan to construct VER-M to evaluate the effect of HSP inhibition on the therapeutic outcome of MPEG-AuNR mediated low temperature PTT. MPEG coated AuNR (MPEG-AuNR) was used as the PTT agent for mild PTT. VER-M and MPEG-AuNR were characterized in detail. Both nano-sized VER-M and MPEG-AuNR could accumulate preferentially in tumor tissues through the EPR effect after intravenous injection as shown in Fig. 1, and then tumor cells were inhibited by a tumor inhibitor and enhanced mild PTT. The tumor inhibiting rate of these systems was further studied *in vitro* and *in vivo*. The inhibition of HSP70 and HSP90 expression was studied by western blot. To summarize, MPEG-AuNR@VER-M is a promising strategy for tumor inhibition.

2. Materials and methods

2.1. Materials

Sodium borohydride (NaBH4), ascorbic acid, tetrachloroauric acid ($HAuCl_4 \cdot 3H_2O$), silver nitrate ($AgNO_3$), *N*-cetyltrimethylammonium bromide (CTAB), DAPI, methyl thiazolyltetrazolium (MTT)

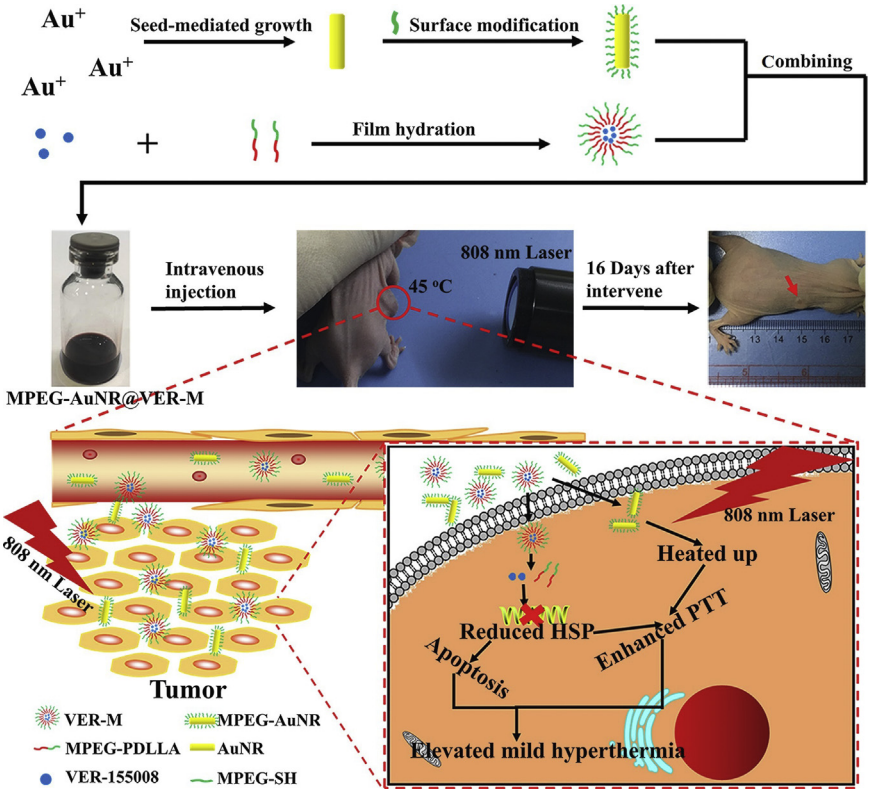

Figure 1 Schematic illustration of MPEG-AuNR@VER-M for tumor apoptosis and selectively sensitizing tumor cells to mild PTT by inhibiting the expression of HSP.

and coumarin-6 (C6) were purchased from Sigma-Aldrich. Inhibitor VER-155008 was purchased from ApexBio. Copolymer MPEG-thiol (5 kDa) was obtained from Ziqi bio company (Shanghai, China). Methoxy poly (ethylene glycol) (MPEG-OH, $M_n = 2000$) was purchased from Sigma–Aldrich (Saint Louis, USA). D,L-Lactic acid (DLLA) was provided by Jinan Daigang Biomaterial Co., Ltd. 1,1-DioCtadecyl-3,3,3,3-tetramethylindodicarboCyanine (DID) was obtained from KeyGen Biotech (Nanjing, China). HSP90 and HSP70 human monoclonal antibodies were obtained from Labvision (Minneapolis, USA). 1640 medium, penicillin-streptomycin liquid (100 ×) and fetal bovine serum (FBS) were obtained from HyClone (Logan, USA). Dichloromethane (DCM) was purchased from Tianjin Bodi Chemical Co., Ltd. (Tianjin, China). Dimethyl sulphoxide (DMSO) was purchased from Tianjin Kermal Chemical Co., Ltd. (Tianjin, China). Chloroform was purchased from Tianjin Fuyu Fine Chemical Co., Ltd. (Tianjin, China). Ethanol was purchased from Aladdin (Shanghai, China).

HCT116 cells were supplied by American Type Culture Collection (ATCC; Rockville, MD, USA), which were grown in a 1640 supplement with 10% FBS, 100 U/mL penicillin and 100 mg/mL streptomycin, respectively. The cell cultures were maintained in a 37 °C incubator with a humidified 5% CO_2 atmosphere.

Female BALB/c mice (20 ± 2 g) were from HFK Bioscience Co., Ltd. (Beijing, China) and kept under SPF conditions with free access to standard food and water. All animal procedures were performed following the protocols approved by the Institutional Animal Care and Treatment Committee of Sichuan University (Chengdu, China).

2.2. *Preparation and characterization of (VER-155008)-loaded micelles*

Briefly, VER and copolymers MPEG-PDLLA (M_n: 4 kDa)[40] were co-dissolved in 2 mL of dehydrated alcohol and placed in a round-bottomed flask. Then the solvent was evaporated in a rotary evaporator at 60 °C for 2 h. Subsequently, the mixture was hydrated with 5 mL water under moderate shaking at 60 °C, and VER-loaded micelles formed by self-assembly. Finally, the micelles were filtered through a syringe filter (pore size: 220 nm) (Millex-LG, Millipore Co., USA), aiming at removing non-entrapped drugs and lyophilized for further applications. The shape and dispersion of the micelles were observed by transmission electron microscope (TEM). The size and zeta potential were detected by dynamic light scattering (Nano-ZS 90, Malvern Instruments, Malvern, UK) at a constant temperature of 25 °C.

The drug release behaviors of the VER micelles of VER-M were determined as follows[73]. Briefly, free VER and VER-M were separately suspended in a dialysis bag (molecular weight cutoff: 14 kDa) and were then immersed into PBS (pH = 7.4) solution at 37 °C under horizontal shaking (100 rpm, HZQ-C, Harbin Donglian Electronic Technology Development Co., Ltd, Harbin, China). At predetermined intervals, the aliquots (2 mL) were withdrawn and replaced by the same amount of PBS. The amount of VER released at designated time points were measured by HPLC.

2.3. *Synthesis of MPEG-AuNR*

Synthesis of AuNR was according to a modified seed-mediated method[61]. Briefly, 7.5 mL CTAB (0.1 mol/L) was mixed with

100 μL $HAuCl_4$ (0.024 mol/L), and 1.8 mL deionized water was added to the mixture. Further, 0.6 mL $NaBH_4$ solution (0.01 mol/L, 4 °C) was added, and stirred continuously for 3 min until the solution became bronze-colored. The solution was then left for 2 h at 25 °C allowing the seeds to grow. Following this, 100 mL CTAB was mixed with 2.04 mL $HAuCl_4$ while stirring vigorously. Then, 2 mL 0.5 mol/L H_2SO_4, 0.9 mL 0.01 mol/L $AgNO_3$ and 0.8 mL 0.1 mol/L ascorbic acid were added to the mixture in turn to prepare a growth solution. A seed solution (240 μL) was added to the solution, which was set overnight at 25 °C. To reduce excess CTAB, the AuNR as-synthesized was purified by centrifugation (16,000 × g, 10 min). To prepare MPEG-AuNR, 100 mg MPEG-thiol (5 kDa) was added to the AuNR solution (10 mL). After stirring for 12 h, the MPEG-AuNR solution was purified by centrifugation (16,000 × g, 10 min).

TEM was used to observe the pattern of AuNR and MPEG-AuNR. The diameter and zeta potential of AuNR and MPEG-AuNR were analyzed by dynamic light scattering (Nano-ZS 90, Malvern Instruments, Malvern, UK) at a constant temperature of 25 °C. Fourier Transform infrared spectroscopy (FTIR) was also used to confirm the successful modification on MPEG-AuNR. The temperature-rising curves of AuNR and MPEG-AuNR at the concentration of 50 mg/L were characterized by different powers of 808 nm NIR laser. Finally, MPEG-AuNR was mixed with VER-M in different ratios before being used. Infrared spectrum was used to observe the successfully modification of gold nanorods.

2.4. Cell culture

Human colon cancer cells (HCT116) were incubated in a 1640 medium with 10% FBS and 1% antibiotics at 37 °C in a humidified atmosphere containing 5% CO_2. Mouse embryonic fibroblasts (3T3) were incubated in a DMEM medium with 10% FBS and 1% antibiotics at 37 °C in a humidified atmosphere containing 5% CO_2.

2.5. In vitro uptake of VER-M

To investigate the uptake of VER-155008 micelles in HCT116, fat-soluble fluorescent molecules coumarin-6 (C6) was used as substitute for VER-155008 in the uptake study. In brief, HCT116 cells were seeded in 6-well plates at a density of 10^5 per well. After 24 h incubation, cells were treated with NS, 100 ng/L of C6 or 100 ng/L of C6 at 45 °C. Ten minutes later, cells were collected and used for fluorescence imaging after DAPI treatment or flow cytometry to observe the localization of C6.

2.6. In vitro cytotoxicity assay

The cytotoxicity of free VER, VER-M, and MPEG-AuNR with VER-M were investigated in HCT116 cells and 3T3 cells. Firstly, cells were seeded in a 96-well plate (6.0×10^3 cells per well) and incubated in 200 μL of 1640 (for HCT116) or DMEM (for 3T3) medium for an additional 24 h. After that, cells were exposed to various concentrations of free VER, MPEG-AuNR, VER-M, and MPEG-AuNR with VER-M with or without NIR laser. After incubation for 12 h, the cell viability was measured by the MTT method. The relative cell viability was calculated as $(OD_{570\ sample}/OD_{570\ control}) \times 100\%$, where $OD_{570\ control}$ was obtained in the absence of therapeutic agents and a $OD_{570\ sample}$ was obtained.

2.7. Live/dead cell staining assay

HCT116 cells were seeded in 6-well plates at a density of 5×10^5 cells per well. After 24 h plating, the cells were incubated with (1) 0, 5 and 10 mg/L VER-M at 37 °C; (2) 0, 5 and 10 mg/L VER-M at 40 °C; (3) 0, 5 and 10 mg/L VER-M containing 50 mg/L MPEG-AuNR with 808 nm Laser (2.5 W/cm^2, 4 min to 45 °C) after being incubated for 2 h; (4) 0, 5 and 10 mg/L VER-M containing 50 mg/L MPEG-AuNR with 808 nm Laser (3 W/cm^2, 4 min to 55 °C), respectively. After incubation for 2 h, the cells were washed 3 times with PBS, and 200 mL working solution (PBS containing 2 μmol/L calcein AM, 8 μmol/L PI) were added and the cells were further incubated for 30 min at room temperature away from light. Finally, the cells were washed 3 times with PBS again, and observed under fluorescent microscopy.

2.8. Evaluation of apoptosis by flow cytometry

HCT116 cells were seeded in 6-well plates at a density of 5×10^6 cells per well. After 24 h incubation, cells were exposed to MPEG-AuNR (40 mg/L) with or without VER-M (10 mg/L). Two hours later the culture medium was incubated at 37 °C or treated with NIR light irradiation (2.5 W/cm^2, 2 min to 40 °C, 3 min to 45 °C or 5 min to 55 °C). The cells incubated at 37 °C without any treatment were tested as the negative control. Then apoptosis of the cells was detected by flow cytometry. The synergistic effect between VER-M and PTT was analyzed *via* Jin's formula:

$$q = E_{A+B}/(E_A + E_B - E_A \times E_B) \quad (1)$$

Where q is the combination index; E_{A+B}, E_A, E_B were the efficacies of drug A + B, drug A and drug B, respectively.

2.9. Western blot analysis of HSP70 and HSP90

In brief, HCT116 cells were seeded in a 6-well plate at a density of 5×10^5 per well for 12 h. Then the cells were treated with different conditions: (1) cell incubated at 37 °C, (2) cell treated with 808 nm NIR laser to 40 °C with various concentrations of VER-M, (3) cell treated with 808 nm NIR laser to 45 °C with various concentrations of VER-M, (4) cell treated with 808 nm NIR laser to 55 °C with various concentrations of VER-M. Four hours later, cells were collected and disrupted by RIPA for 10 min. The expression of HSP90 and HSP70 was detected by western blot. The protein expression of HSP70 and HSP90 on the membranes was analyzed by an exposure meter.

2.10. Animals and tumor models

Female BALB/c nude mice (4−5 weeks old) were bought from Beijing HFK Bioscience Co., Ltd (Beijing, China). All animal experiments were performed in agreement with institutional animal use and care regulations from Sichuan University. The tumors were obtained by injecting female mice with HCT116 cells (1.5×10^6 cells) subcutaneously in the right armpit region.

2.11. In vivo tumor-targeted photoacoustic imaging (PAI) and photothermal curves

When tumors reached a size of approximately 150 mm^3 in volume, 200 μL MPEG-AuNR (500 mg/L) or Normal saline (NS as control) was intravenously injected into the tumor-bearing mice.

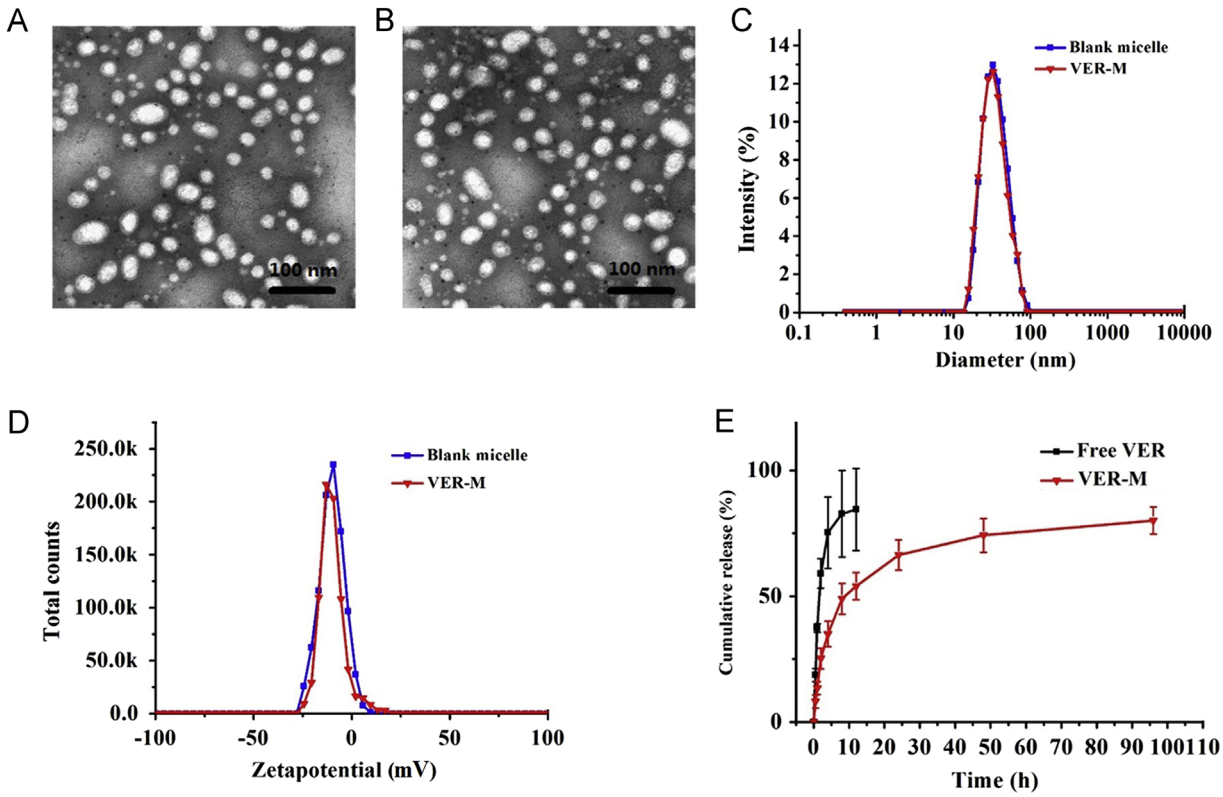

Figure 2 TEM images of blank micelle (A) and VER-M (B). (C) Diameter of blank micelle and VER-M. (D) Zeta potential of blank micelle and VER-M. (E) Drug release curve of Free VER and VER-M.

Images were obtained after 0, 2, 8, 12 and 24 h by PAI. For further study the temperature-rising curve of MPEG-AuNR *in vivo*, mice injected after 12 h were treated with 808 nm NIR laser on their tumors, and then time–temperature curves were drawn/obtained.

2.12. *In vivo fluorescence imaging study*

To investigate the delivery of VER-M *in vivo*, real-time fluorescence imaging was carried out. 1,1-DioCtadecyl-3,3,3,3-tetramethylindodicarboCyanine (DID) was replaced VER as the fluorescence probe to be wrapped in micelles. Normal saline, free DID, DID micelles, DID micelles and MPEG-AuNR (treated with PTT to 45 °C) were intravenously injected into the tumor-bearing mice until the tumor volume reached approximately 200 mm^3. Fluorescence imaging was observed at predestined time intervals (2 h, 4, 8, 12, and 24 h). Further to investigate the biodistribution of VER in the mice, tumors and other main organs (liver, spleen, lung, kidney, and heart) were harvested 12 h after injection.

2.13. *In vivo antitumor effect*

When the tumors reached a size of 200 mm^3, the tumor bearing mice were divided into 7 groups: (1) NS group as control; (2) 10 mg/kg VER-M; (3) mice injected with 5 mg/kg MPEG-AuNR (treated with PTT to 40 °C) (4) mice injected with 5 mg/kg MPEG-AuNR and 10 mg/kg VER-M (treated with PTT to 40 °C); (5) mice injected with 5 mg/kg MPEG-AuNR (treated with PTT to 45 °C); (6) mice injected with 5 mg/kg MPEG-AuNR and 10 mg/kg VER-M (treated with PTT to 45 °C); (7) mice injected with 5 mg/kg MPEG-AuNR (treated with PTT to 55 °C), respectively. The weight of the mice and tumor volume was measured every other day. Tumor sizes were measured by caliper, and tumor volume was calculated[74] as (tumor width)^2 × (tumor length)/2. The tumor inhibiting rate was calculated as $V/V_{control}$. The synergistic effect between VER-M and PTT was analyzed *via* Jin's formula:

$$q = E_{A+B}/(E_A + E_B - E_A \times E_B) \quad (2)$$

where q was the combination index; E_{A+B}, E_A, E_B were the efficacies of drug A + B, drug A and drug B, respectively). Relative body weight was determined as W/W_0 (W_0 is the body weight before therapy). Five mice in each group were used to observe survival times. Moreover, the tumor tissues were treated with H&E staining to observe tumor apoptosis.

2.14. *Statistical analysis*

Statistical significance was analyzed by a three-sample Student's test. Statistical significance was inferred at a value of $P < 0.05$.

3. Results

3.1. *Preparation and characterization of VER-M and MPEG-AuNR*

TEM displayed the shape and dispersion of blank micelles and VER-M (Fig. 2A and B). The particle sizes of VER-M and blank micelles were around 30 nm (Fig. 2C). The polydispersity index (PDI) of VER-M and the blank micelles were about 0.13, which

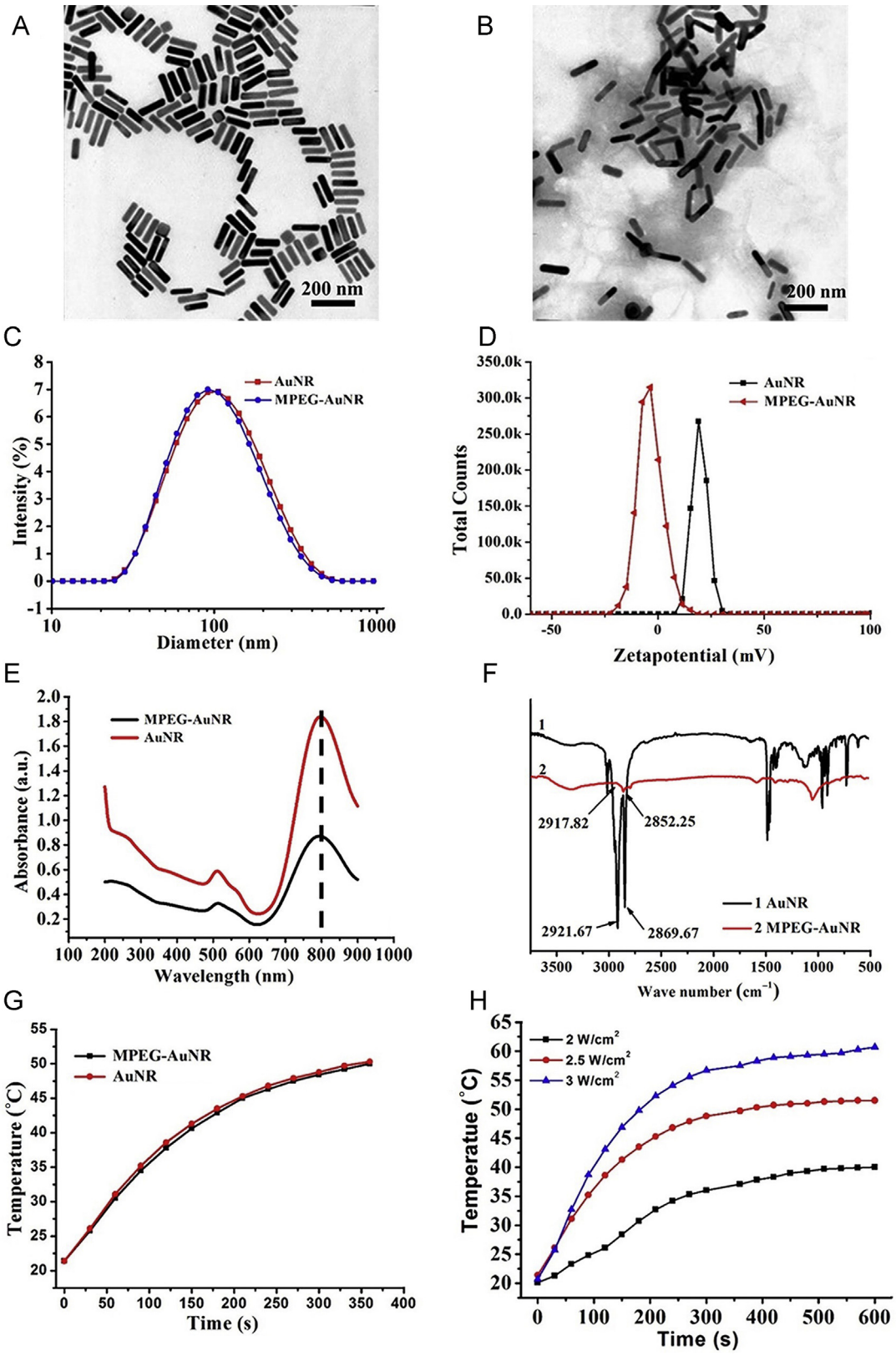

Figure 3 TEM images of AuNR (A) and MPEG-AuNR (B). (C) Diameter of AuNR and MPEG-AuNR. (D) Zeta potential of MPEG-AuNR and AuNR. (E) The absorption spectrum of MPEG-AuNR and AuNR. (F) The IR spectra of MPEG-AuNR and AuNR. (G) Heating curves of MPEG-AuNR and AuNR at the concentration of 50 mg/L with fixed 2.5 W/cm^2 808 nm laser power. (H) Heating curve of MPEG-AuNR at the fixed concentration of 50 mg/L with different 808 nm laser powers.

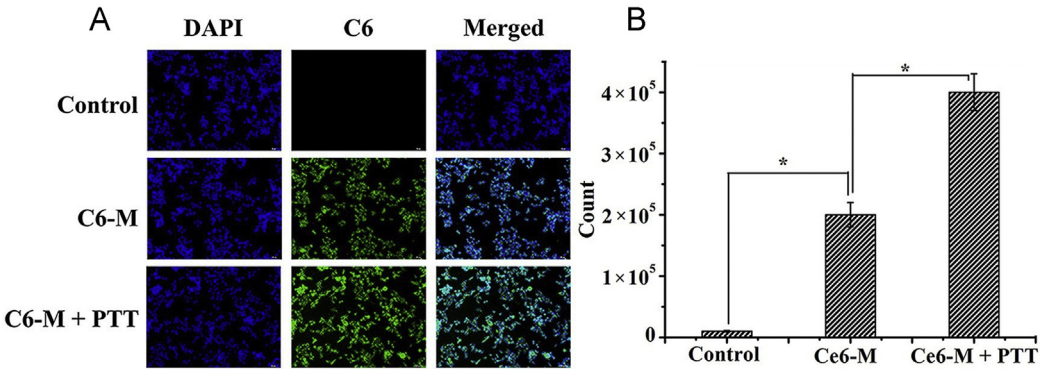

Figure 4 (A) Fluorescent microscopy images of HCT116 cells with different treatments (scale bar: 20 μm) and (B) Flow cytometry measurement of C6 levels in HCT116 (*$P < 0.05$).

showed narrow and normal distribution. The zeta potential of VER-M and blank micelles was around −10 mV (Fig. 2D). All these results proved that the solubility of VER could be improved by being entrapped in the micelles. As displayed in Fig. 2E, approximate 75% of VER was released from MPEG-PDLLA micelles after 24 h, which provided an opportunity for the inhibitor's release. Moreover, mixing the MPEG-AuNR with VER-M also had a good dispersion and passed through a 450 nm filter.

Rod shaped AuNR (98 nm in diameter) was prepared as the heat generator for PTT (Fig. 3). The transmission electronic microscopy (TEM) images (Fig. 3A and B) showed the good dispersion of AuNR in solution with or without MPEG, and their diameters were around 70 nm (Fig. 3C) and PDI were around 0.3. The zeta potential of the AuNR (34.16 mV) and the MPEG-AuNR (−3.2 mV) (Fig. 3D) indicated that the CTBA on AuNR had been replaced by MPEG-SH, and the AuNR had been coated by MPEG successfully. As was shown in Fig. 3F, strong absorption peaks at 2921.67 and 2869.67 cm^{-1} which belong to C–H stretch vibration[40] were observed in AuNR. While absorption peaks at 2917.82 and 2852.25 cm^{-1} in MPEG-AuNR became much weaker, which proved that the CTAB surfactant has been replaced by MPEG-SH. This result was consistent with the zeta pontential, and all these results confirmed the successful surface modification of AuNR.

The absorption spectrum peak at 800 nm was observed both in AuNR and MPEG-AuNR (Fig. 3E), so that both AuNR and MPEG-AuNR were photothermally stimulated by a 808 nm near-infrared laser. There were no significant differences between the heating curve of AuNR and that of MPEG-AuNR (Fig. 3G), coating with MPEG could not reduce the photothermal effect of AuNR. Heating curves of MPEG-AuNR with different 808 nm NIR laser powers at the concentration of 50 mg/L (Fig. 3H) showed that the end heating temperature was related to time and laser power, which gave guidance for the measure to get different temperatures. In conclusion, MPEG-AuNR with a photothermal effect has been prepared successfully.

3.2. *In vitro uptake study*

Cell uptake of the micelles in HCT116 is shown in Fig. 4. The VER was replaced by C6 as the fluorescence probe to explore the cell uptake in HCT116. In Fig. 4A, no green fluorescence can be seen in the NS group, and strong fluorescence can be observed in the micelle group, which indicated that the micelles could be taken up by HCT116. Besides, the fluorescence intensity in the C6-M+PTT group was stronger than in the C6-M group. The quantitative analysis of cell uptake ratio was detected by flow cytometry. In Fig. 4B, the fluorescence intensities of the micelle groups are significantly stronger than the NS groups, and this result was consistent with the fluorescence observation. These results indicate that the micelles could deliver the hydrophobic drugs into cells *in vitro*.

3.3. *Inhibition of tumor growth in vitro*

Next, the synergistic effect of VER and photothermal therapy (PTT) for inhibiting the growth of tumor cells by AuNR and VER-M was investigated in this series of experiments *in vitro*, and the results are summarized in Fig. 5. As shown in Fig. 5A, viabilities of HCT116 were over 85% in free VER groups at concentrations from 0 to 160 mg/L. The cytotoxicity of the VER-M depended on the dose concentration of VER which was more effective than free VER. These results indicated that loading VER into MPEG-PDLLA micelles could improve the inhibition of the growth of HCT116 cells.

As shown in Fig. 5B, the synergistic inhibition effects of VER-M and PTT for HCT116 were investigated. With the increase of the PTT temperature, the viability of HCT116 decreased. However, it was easy to observe in individual PTT groups that the viabilities were all above 50% except for the 55 °C group. So individual mild PTT could not inhibit the tumor cell growth effectively. On the other hand, the viability of the cells was decreased remarkably when the cells were treated with PTT and VER-M, and this depended on the dose of VER. In combined therapy groups, the cell viabilities were less than 10% at 45 °C, and there were no significant differences compared to the group treated with 10 mg/L at 55 °C. Therefore, these results indicated that VER-M could effectively enhance mild PTT, and in this article, the 55 °C group would act as the positive control group. In conclusion, MPEG-AuNR was a kind of biosafe and effective PTT agent; the rate of HCT116 growth inhibition by VER-M depended on the dose of VER. Combining PTT and VER-M in tumor therapy treatment could enhance the anti-tumor effect.

The biocompatibilities of MPEG-AuNP and VER-M were investigated in 3T3 cells, as displayed in Fig. 5C, the viabilities of 3T3 cells treated with MPEG-AuNR were over 85%, since the

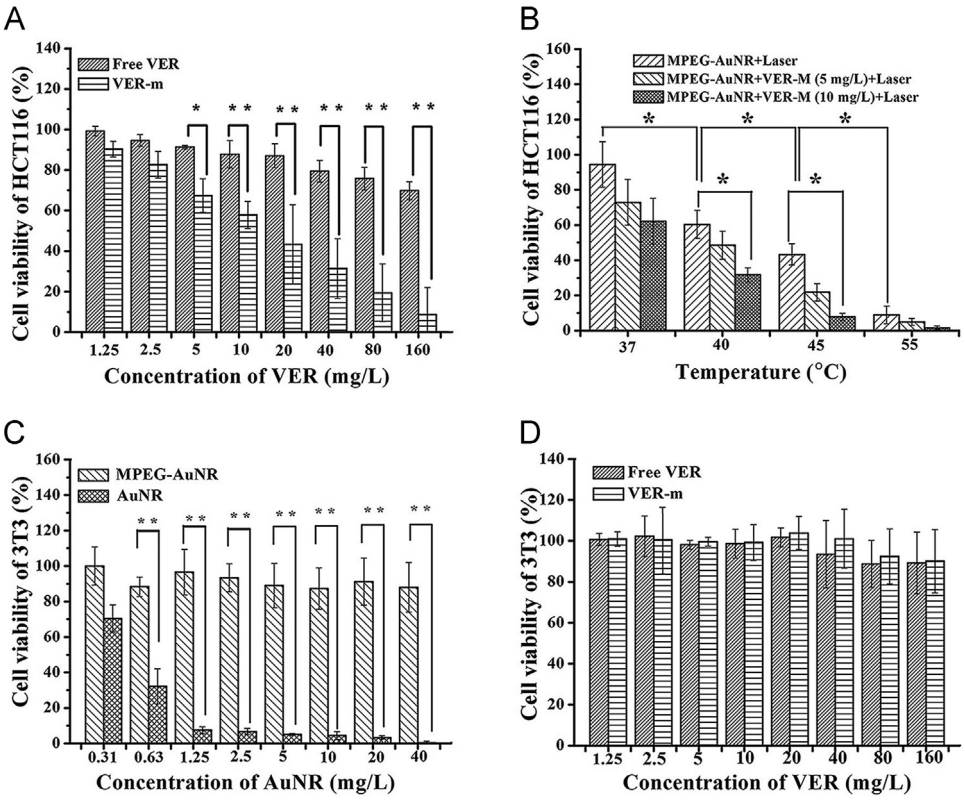

Figure 5 Cytotoxicity of (A) free VER or VER-M against HCT116 ($^{*}P<0.05$ and $^{**}P<0.005$), (B) MPEG-AuNR combining with different concentrations of VER-M at different PTT temperatures against HCT116 ($^{*}P<0.05$), (C) MPEG-AuNR or AuNR against 3T3 ($^{**}P<0.005$), (D) free VER or VER-M against 3T3.

concentration of AuNR was up to 0.625 mg/L. Therefore, the biocompatibility of AuNR could be improved by modifying MPEG on the surface of AuNR. The biocompatibilities of VER-M for normal cells were observed in Fig. 5D. These results illustrated that the HCT116 cells were more sensitive than the normal cells to VER-M.

3.4. *Live/dead cell and apoptosis*

According to the live/dead cell images which are shown in Fig. 6A, the live cells had an overall majority at 37 °C even in the 10 mg/L of VER-M. With the increasing concentration of VER-M, the death ratios of cells increased at 40 °C. However, there were about 40% live cells even when the concentration of VER-M was up to 10 mg/L. Continuously, at a temperature of 45 °C, the percentage of dead cells was almost 100% when treated with 10 mg/L VER-M; while at 55 °C, the dead cells had an overall majority in any concentration of VER-M, and these results were consistent with the MTT assays. Live/dead analysis proved that both raising temperature and raising dosage of VER-M could improve the death ratio of HCT116 cell *in vitro*, and 10 mg/L might be an ideal dose.

Apoptosis rates of HCT116 were evaluated further by flow cytometry (Fig. 6B). The apoptosis ratios of different groups were control, 0%; 10 mg/L VER-M at RT, 46.82%; 0 mg/L VER-M at 40 °C, 44.20%; 10 mg/L VER-M at 40 °C, 71.45%; 0 mg/L VER-M at 45 °C, 48.99%; 10 mg/L VER-M at 45 °C, 76.56%; 0 mg/L VER-M at 55 °C, 63.52%; 10 mg/L VER-M at 55 °C, 86.60%, respectively. By the introduction of laser irradiation or VER-M, the apoptosis was further promoted (Fig. 6B). Under the VER-M/PTT combination therapy, the synergetic indexes were 1.05 and 1.03, in the 40 °C and 45 °C group, respectively. It indicated that the PTT and VER-M formed a synergistic effect in HCT116 cells apoptosis. However, tumor apoptosis rates of cells treated at 40 °C were relatively low, which indicated that PTT was ineffective at 40 °C even with VER-M. To summarize, 45 °C was observed as the optimum mild PTT temperature in these studies.

3.5. *In vitro Western blot (WB) study*

To demonstrate the link between apoptosis and the HSP inhibitor, the protein expression of HSP70 and HSP90 were studied with different doses of VER and temperatures of PTT as shown in Fig. 7. In groups at a temperature of 40 °C (Figs. 7A and 7D), the HSP expression of cells decreased with the concentration of VER-M increased. Similarity in 45 °C groups (Fig. 7B and E), HSP expression was prevented with the increasing dose of VER-M. Also similar results could be observed in 55 °C groups (Fig. 7C and F), HSP expression positively correlated with VER-M. Expression of HSP in the individual PTT groups was higher than the control group. These results indicate that high temperature promoted the expression of HSP. In consequence, VER-M could suppress the expression of HSP90 and HSP70 as the environmental temperature rose.

3.6. *In vivo tumor-targeted photoacoustic imaging (PAI)*

The targeting efficiency of MPEG-AuNR in solid tumors was evaluated by PAI. The presence of MPEG-AuNR increased in

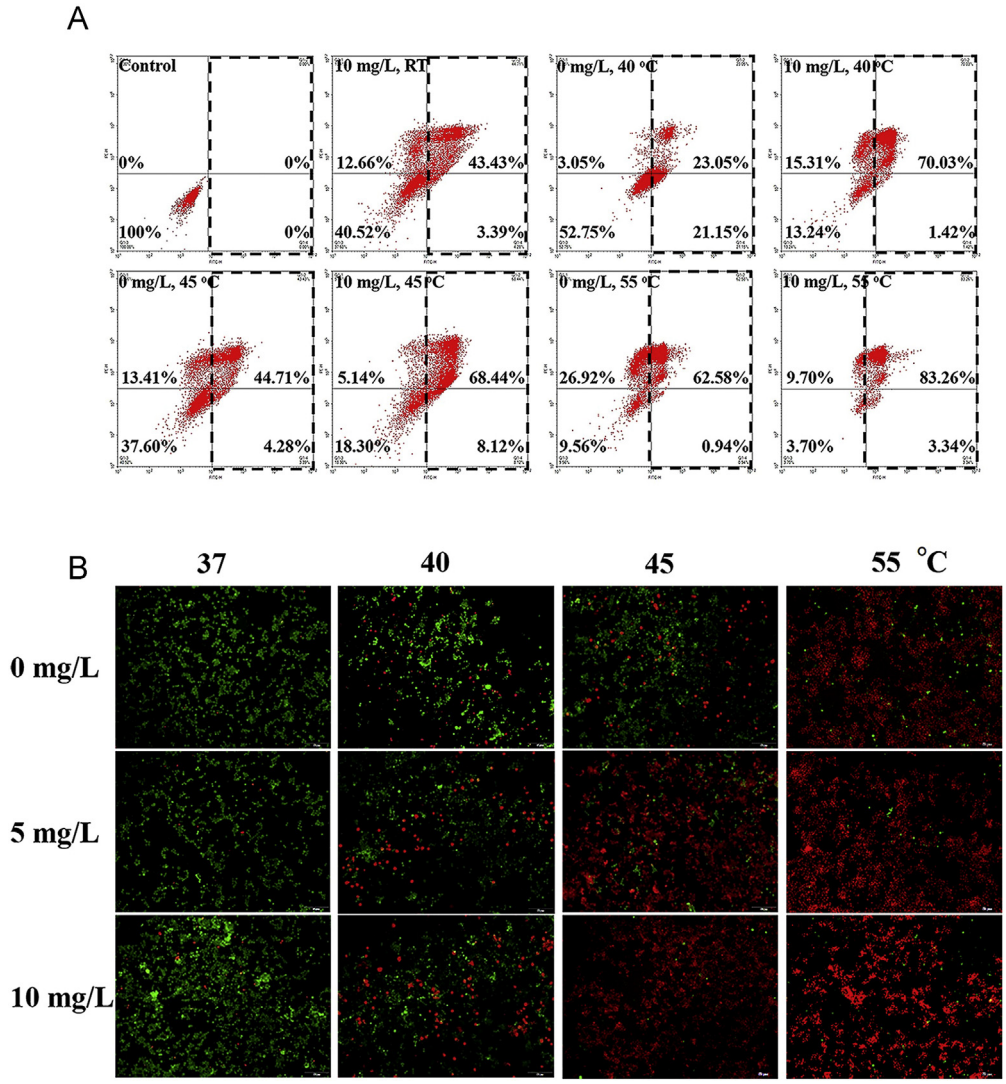

Figure 6 (A) Fluorescence live/dead cell images of HCT116 cells with different concentrations of VER-M and PTT temperatures. Scale bar: 50 μm. (B) Flow cytometry analysis of apoptosis and necrosis of HCT116 cells with different concentrations of VER-M and PTT temperatures.

the tumor site as time passed (Fig. 8A and B), and concentrations of AuNR were linear with PAI signals. In particular, the concentration of MPEG-AuNR in the tumor reached a max at 12 h after injection. The intensity of the signal in the tumor was much stronger than other tissues. This phenomenon illustrated that MPEG-AuNR could concentrate in the tumor side, and suggested 12 h after injection may be the best time for PTT.

Furthermore, the heating curve *in vivo* at 12 h after injection was studied (Fig. 8C and D), and the mice injected with NS were considered as control. The temperature around the tumors in the MPEG-AuNR group rose as time went on. Especially, 40–42 °C was achieved after 1 min's laser treatment, 45–47 °C was achieved after 2 min's laser treatment, and 55–57 °C was achieved after 5 min's laser treatment. In contrast, the tumor temperature in the control group was kept at normal body temperature. All these studies showed MPEG-AuNR could make the tumor temperature increase by introducing the laser radiation.

3.7. *In vivo fluorescence imaging*

To confirm the *in vivo* tumor-targeted efficiency of VER-M, DID as the fluorescence probe to replace VER was explored *in vivo*, and the results were displayed in Fig. 9. Two hours after injection, the fluorescence in experimental groups could be seen *in vivo*. Fluorescence intensity in the free DID group weakened after 12 h, whereas in the micelle groups it strengthened in the tumor site. This indicated that micelles could reduce the clearance rate of drugs *in vivo*, and concentrate in the tumor site through the EPR effect. Furthermore, comparing the group c (DID-M without PTT) with the group d (DID-M with PTT), the intensity of DID-M in the group c's tumor was weaker. This result indicated that the PTT might promote the enrichment of micelles in the tumor side, which because hyperthermia can overcome multidrug resistance (MDR)[78]. Although the exact mechanism is still unclear, it is true that hyperthermia can affect transmembrane conductivity, sodium/potassium-ATPase activity, glutathione metabolism and P-glycoprotein (P-gp) activity[79]. Because the strongest fluorescence intensity appeared at 12 h after administration, the PTT was carried out after the injection of MPEG-AuNR@VER-M at 12 h for further research.

3.8. *Anti-tumor in vivo*

Encouraged by the favorable therapeutic effect *in vitro* and the satisfactory NIR-induced photothermal conversion result *in vivo*,

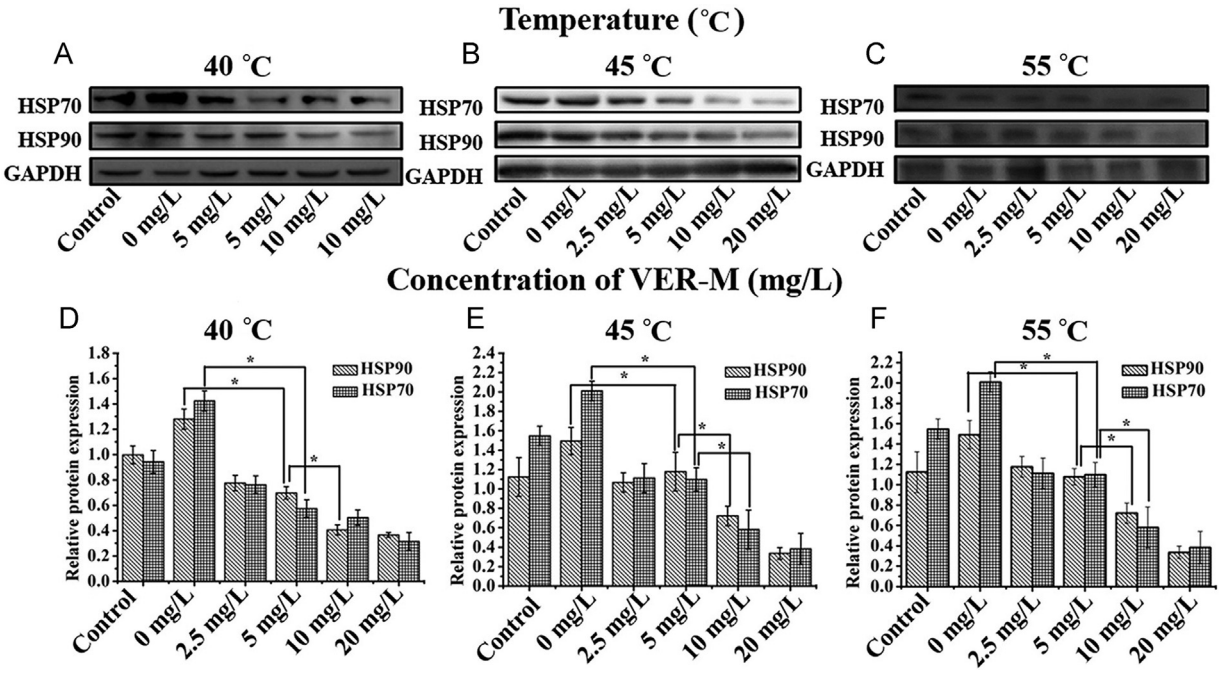

Figure 7 Western blot images of HTC116 treated with (A) different concentration of VER-M at 40 °C, (B) different concentrations of VER-M at 45 °C, and (C) different concentrations of VER-M at 55 °C. Relative HSP90 and HSP70 protein expression of HCT116 treated with (D) different concentrations of VER-M at 40 °C (*$P<0.05$), (E) different concentrations of VER-M at 45 °C (*$P<0.05$) and (F) different concentrations of VER-M at 55 °C (*$P<0.05$). HCT116 incubated at 37 °C without VER-M was control in (A), (B), (C), (D), (E) and (F).

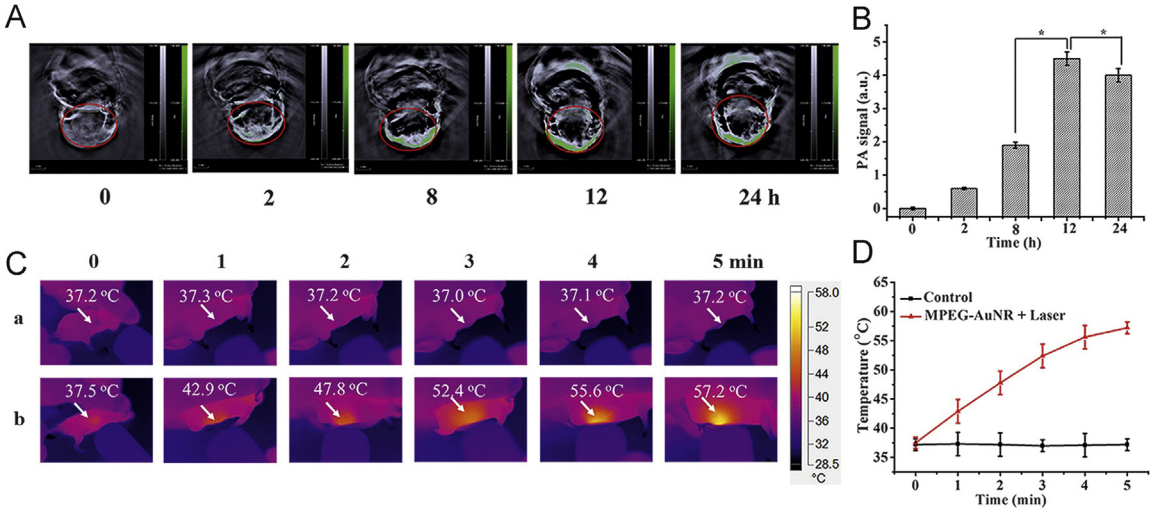

Figure 8 (A) PA images of mice at 0, 2, 8, 12 and 24 h after being injected with MPEG-AuNR. (B) PA signal of mice at 0, 2, 8, 12 and 24 h after being injected with MPEG-AuNR (*$P<0.05$). (C) *In vivo* photothermal images of mice after intravenous injection of NS (a) and MPEG-AuNR (b). (D) Temperature increase curve of the NIR-laser-irradiated tumor tissues as a function of irradiation time.

the antitumor effect of MPEG-AuNR@VER-M was further investigated *in vivo*. The tumor growth curves after administration are shown in Fig. 10A, the significant difference between groups with or without PTT, which indicated that the PTT was more effective than the individual VER-M group for tumor therapy. Also, among the individual PTT group, tumor growth inhibition increased as the temperature rose. Moreover, compared with the synergistic group, the individual PTT group exhibited weaker inhibition for tumor growth, so that the VER-M could promote the anti-tumor effect of PTT *in vivo*. It was easily observed that there were no significant differences between tumor volumes of the MPEG-AuNR@VER-M 45 °C group and MPEG-AuNR 55 °C group 16 days after administration, and the tumor had almost disappeared. The images of mice at real-time points and the isolated tumors at 16 days are displayed in Fig. 10D and E. Furthermore, to investigate the anti-tumor effects of different formulations, H&E stain was used for detecting the tumor cell damage (Fig. 11). The most serious damage appeared in the

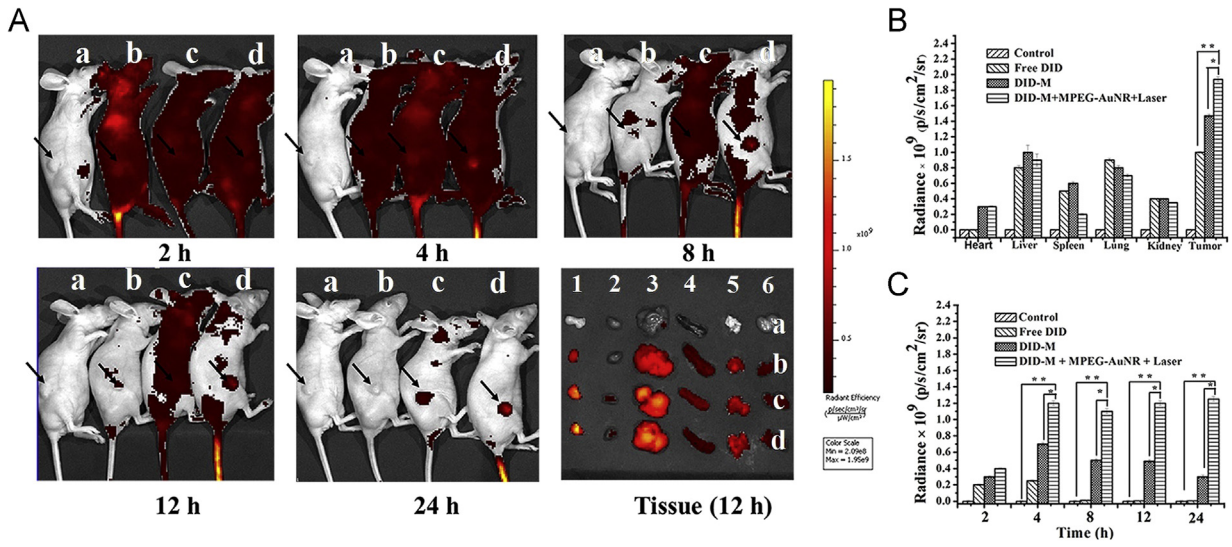

Figure 9 (A) *In vivo* fluorescence imaging at different times after injection. (a) NS as control, (b) free DID; (c) DID-M; (d) MPEG-AuNR@DID-M with PTT, respectively. In A, the arrow head points toward tumor tissue, and 1, 2, 3, 4, 5, and 6 are tumor, heart, liver, spleen, lung, kidney, respectively. The quantitative analysis of the fluorescence intensity in mice and in tissues (*$P<0.05$, ** $P<0.005$) are shown in (B) and (C).

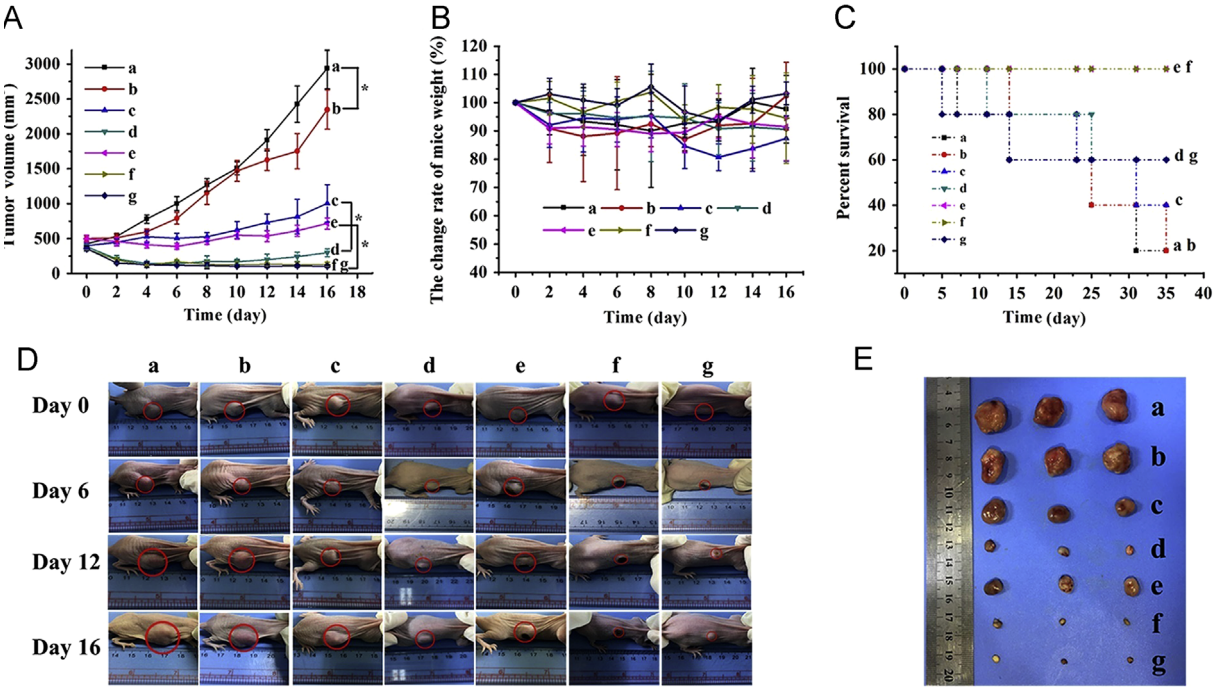

Figure 10 *In vivo* antitumor study after injection. (a) NS as control, (b) VER-M; (c) MPEG-AuNR with PTT at 40 °C; (d) MPEG-AuNR@VER-M with PTT at 40 °C; (e) MPEG-AuNR with PTT at 45 °C; (f) MPEG-AuNR@VER-M with PTT at 45 °C; (g) MPEG-AuNR with PTT at 55 °C. (A) Tumor volumes after different treatments. (B) Relative body weight after different treatments. (C) Survival curves of different treatments. (D) The photograph of the mice with different treatments at 0, 6, 12 and 16 days after administration. (E) Photographs of tumor tissues 16 days after injection.

MPEG-AuNR@VER-M 45 °C and MPEG-AuNR 55 °C group. Also, the survival time of the mice was investigated for 35 days after administration. As shown in Fig. 10C, no mice from group e (tumor treated with PTT at 45 °C alone) and f (tumor treated with 10 mg/kg VER-M and PTT at 45 °C) died (Fig. 10C), while only 60% of the mice of group g (tumor treated with PTT at 55 °C alone) died, owing to recurrence of the tumors. These results indicated that PTT combined with VER-M had less recurrence rate than hyperthermia. This results because heatstroke not only directly induces cell injury, but also causes the release of large

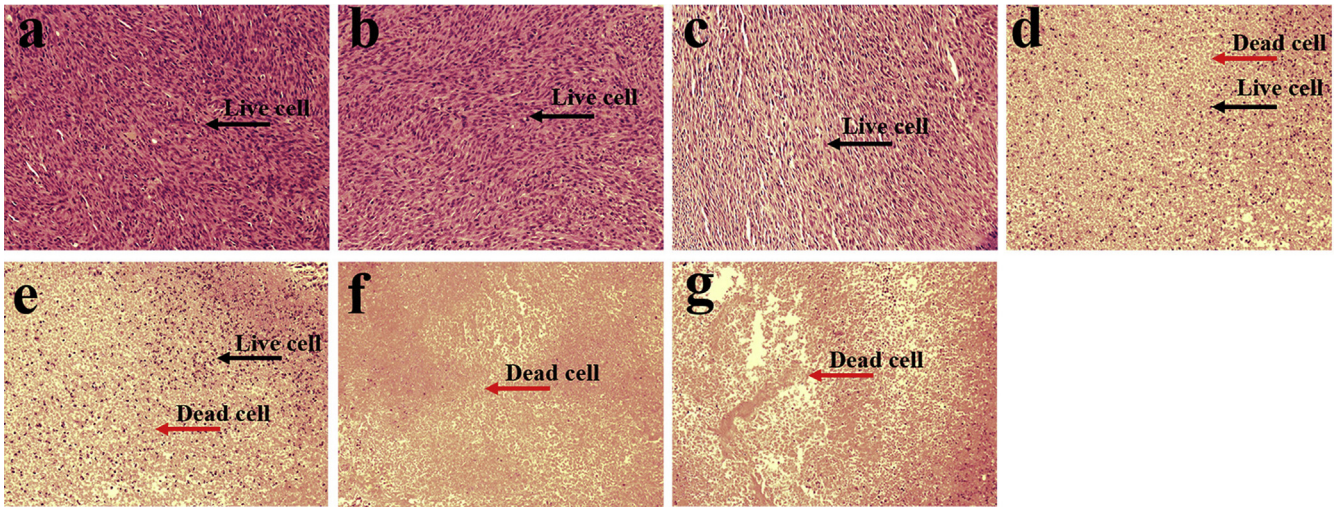

Figure 11 Effect of PTT on the tumors from HCT116 tumor-bearing mice from (a) NS as control, (b) VER-M; (c) MPEG-AuNR with PTT at 40 °C; (d) MPEG-AuNR@VER-M with PTT at 40 °C; (e) MPEG-AuNR with PTT at 45 °C; (f) MPEG-AuNR@VER-M with PTT at 45 °C; (g) MPEG-AuNR with PTT at 55 °C.

amounts of inflammatory mediators and cells with extensive biological activities to induce a systemic inflammatory response and immune dysfunction, which has been widely studied[62–72]. The biocompatibility of the formulation was reflected by the weight change during the treatment. There was no dramatic reduction in each group, indicating that MPEG-AuNR@VER-M was a safe formulation in tumor therapy. In conclusion, these results indicated that combining MPEG-PDLLA with the small molecular inhibitor VER in tumor therapy, not only could improve the anti-tumor effect of PTT, but also make mild PTT become reality.

4. Discussion

PTT is an efficient therapeutic process with low side-effects for cancer therapy[40,41], which specifically ablate cancer at tumor tissue. However, many challenges such as inflammatory response, immune dysfunction and penetration depth[59,62–72] are needed to be considered. As was mentioned in this study, PTT can be divided into hyperthermia ($>$ 45 °C) and mild PTT ($\leq$ 45 °C)[53]. High photothermal therapy may become unrealistic *in vivo* due to the unsatisfied penetration depth in biological tissues of NIR. Just as important, aggrandized side-effects to the surrounding tissue near tumors[62–72] are also considered to be a grievous problem.

Although there were some studies aimed at improving the photo-thermal conversion rate in deep tissue,[59] mild PTT still seems to be the relatively easy method for tumor photothermal therapy. The main problem of mild PTT was the low therapy effect due to the thermotolerance because of high expression of HSPs protein in cancer cells. Many studies in the past aimed at improving PTT by combining PTT with chemotherapy[74,75], which with high requirement of the materials in drug delivery systems and were only proposals for the certain given environment or some target condition. HSPs play the key role in activating thermotolerance in hyperthermia therapy, and several nanosystems were developed to sensitize tumor cells by using HSP inhibitors or siRNA to enhance therapeutic efficiacy both *in vitro* and *in vivo*[18]. In this study we demonstrated that combining VER-M with PTT could enhance the efficiency of mild PTT, which indicated that MPEG-AuNR@VER-M was an effective method to enhance mild PTT in which VER-155008 considered to be the PTT sensitizer.

MPEG-AuNR was used as model materials for mild PTT in this study. It is noteworthy that there was no chemical conjugation between VER-M and MPEG-AuNR, which indicated that VER-M as PTT sensitizer might be in common use for other photothermal conversion materials. This materials might including graphene[76], nano Fe_3O_4[77] and so on. We believe that the graphene @VER-M or nano Fe_3O_4@VER-M system would be useful for mild PTT in the future. Or more succinctly, other kinds of heat treatments for cancer therapy such as hot compress[80] and hyperthermic perfusion[81] could be enhanced by forming hot compress@VER-M or hyperthermic perfusion@VER-M system.

5. Conclusions

In this study, we entrapped the small molecule HSP70 and HSP90 inhibitor VER into MPEG-PDLLA to form VER-M. The size of VER-M was around 30 nm, which could be concentrated in the solid site through the EPR effect. In this article, VER-M as the PTT sensitizer combined with MPEG-AuNR to prepare a MPEG-AuNR@VER-M formulation for tumor PTT. MPEG-AuNR as the PTT agent translated NIR to heat. The tumor target property of MPEG-AuNR was exhibited in PAI detection. The tumor inhibition of the therapy system MPEG-AuNR@VER-M has been studied in detail *in vitro* and *in vivo*. These results demonstrated that combining VER-M with PTT could enhance the efficiency of mild PTT, and the mild PTT could reduce side-effects and recurrence rate by PTT at 55 °C. In conclusion, MPEG-AuNR @VER-M was an efficient therapeutic protocol in mild PTT.

Acknowledgments

This work was financially supported by The National Natural Science Fund for Distinguished Young Scholars (NSFC31525009), National Natural Science Foundation of China (31771096), Sichuan Innovative

Research Team Program for Young Scientists (2016TD0004), and Distinguished Young Scholars of Sichuan University (2011SCU04B18).

References

1. Gou ML, Men K, Zhang J, Li YH, Song J, Luo S, et al. Efficient inhibition of C-26 colon carcinoma by *VSVMP* gene delivered by biodegradable cationic nanogel derived from polyethyleneimine. *ACS Nano* 2010;**4**:5573–84.
2. Sun B, Luo G, Cui W, Sun J, He Z. Chemotherapy agent-unsaturated fatty acid prodrugs and prodrug-nanoplatforms for cancer chemotherapy. *J Control Release* 2017;**264**:145–59.
3. Cornelis JAP, Miriam K, Louis V. From tumour heterogeneity to advances in precision treatment of colorectal cancer. *Nat Rev Clin Oncol* 2017;**14**:235–46.
4. Zoi K, Evripidis G, Poulikos IP. New perspectives for targeting RAF kinase in human cancer. *Nat Rev Cancer* 2017;**17**:676–91.
5. Srivastava A, Babu A, Filant J, Moxley KM, Ruskin R, Dhanasekaran D, et al. Exploitation of exosomes as nanocarriers for gene-, chemo-, and immune-therapy of cancer. *J Biomed Nanotechnol* 2016;**12**:1159–73.
6. Leroy S, Harshada P, Amal S. Could the anti-chaperone VER155008 replace temozolomide for glioma treatment. *J Cancer* 2015;**6**:786–94.
7. Wu YZ, Sun J, Zhang YQ, Pu MM, Zhang G, He NY, et al. Effective integration of targeted tumor imaging and therapy using functionalized InP QDs with VEGFR2 monoclonal antibody and miR-92a inhibitor. *ACS Appl Mater Interfaces* 2017;**9**:13068–78.
8. Zhao WN, Qiu YL, Kong DX. Class I phosphatidylinositol 3-kinase inhibitors for cancer therapy. *Acta Pharm Sin B* 2017;**7**:27–37.
9. Tobias O, Piotr S. Cell cycle proteins as promising targets in cancer therapy. *Nat Rev Cancer* 2017;**17**:93–115.
10. Hartland WJ, Virginie D, Paul W, Rama K. TIMPs: versatile extracellular regulators in cancer. *Nat Rev Cancer* 2017;**17**:38–53.
11. Itys C, Eva MR, Benjamin L, Kristian H. Maintaining cell identity: PRC2-mediated regulation of transcription and cancer. *Nat Rev Cancer* 2016;**16**:803–10.
12. Peter JM, Rosemary Y, Joseph L, Michael CA, Linda ZP. The interplay between cell signalling and the mevalonate pathway in cancer. *Nat Rev Cancer* 2016;**16**:718–31.
13. Zhang HY, Jiang W, Liu RL, Zhang J, Zhang D, Li ZH, et al. Rational design of metal organic framework nanocarrier-based codelivery system of doxorubicin hydrochloride/verapamil hydrochloride for overcoming multidrug resistance with efficient targeted cancer therapy. *ACS Appl Mater Interfaces* 2017;**9**:19687–97.
14. Li H, Guo S, Cai L, Ma W, Shi Z. Lipopolysaccharide and heat stress impair the estradiol biosynthesis in granulosa cells *via* increase of HSP70 and inhibition of smad3 phosphorylation and nuclear translocation. *Cell Signal* 2017;**30**:130–41.
15. Manik C, Mindaugas A, Thorsten S, Elisabeth M, Claudia H, Torsten S, et al. The PI3K/Akt signaling pathway regulates the expression of Hsp70, which critically contributes to Hsp90-chaperone function and tumor cell survival in multiple myeloma. *Haematologica* 2013;**98**:1132–41.
16. Fan YJ, Liu Y, Zhang LR, Cai F, Zhu LP, Xu JH. C0818, a novel curcumin derivative, interacts with Hsp90 and inhibits Hsp90 ATPase activity. *Acta Pharm Sin B* 2017;**7**:91–6.
17. Cavanaugh A, Juengst B, Sheridan K, Danella JF, Williams H. Combined inhibition of heat shock proteins 90 and 70 leads to simultaneous degradation of the oncogenic signaling proteins involved in muscle invasive bladder cancer. *Oncotarget* 2017;**6**:39821–38.
18. Chen WH, Luo GF, Lei Q, Hong S, Qiu WX, Liu LH, et al. Overcoming the heat endurance of tumor cells by interfering with the anaerobic glycolysis metabolism for improved photothermal therapy. *ACS Nano* 2017;**11**:1419–31.
19. Wang S, Tian Y, Tian W, Sun J, Zhao S, Liu Y, et al. Selectively sensitizing malignant cells to photothermal therapy using a CD44-targeting heat shock protein 72 depletion nanosystem. *ACS Nano* 2016;**10**:8578–90.
20. Maureen EM. The HSP70 family and cancer. *Carcinogenesis* 2013;**34**:1181–8.
21. Helen AA, Kim YS, Brian EO, Shi ZZ, Rita ES. HSP70 promoter-driven activation of gene expression for immunotherapy using gold nanorods and near infrared light. *Vaccines* 2014;**2**:216–27.
22. Georgios DL, George AA, Alberto M, Alessandro M, Stefano R, Luigi B, et al. The role of heat shock proteins in cancer. *Cancer Lett* 2014;**360**:114–8.
23. Christopher GE, Lyra C, Jason EG. Heat shock protein 70 (Hsp70) as an emerging drug target. *J Med Chem* 2010;**53**:4585–602.
24. Lin TY, Guo WC, Long QL, Ma AH, Liu QQ, Zhang HY, et al. HSP90 inhibitor encapsulated photo-theranostic nanoparticles for synergistic combination cancer therapy. *Theranostics* 2016;**6**:1324–5.
25. Moustafa RKA, Hala RA, Carl RR, Mostafa AE. Targeting heat shock protein 70 using gold nanorods enhances cancer cell apoptosis in low dose plasmonic photothermal therapy. *Biomaterials* 2016;**102**:1–8.
26. Gaëtan J, Adonis H, Renaud S, Carmen G. Targeting heat shock proteins in cancer. *Cancer Lett* 2013;**332**:275–85.
27. Dai Z, Tu Y, Zhu L. Multifunctional micellar nanocarriers for tumor-targeted delivery of hydrophobic drugs. *J Biomed Nanotechnol* 2016;**12**:1199–210.
28. Mao J, Tang S, Hong D, Zhao F, Niu M, Han X, et al. Therapeutic efficacy of novel microwave-sensitized mPEG-PLGA@ZrO2@(DOX+ILS) drug-loaded microspheres in rabbit VX2 liver tumours. *Nanoscale* 2017;**9**:3429–39.
29. Chen XL, Liu LS, Jiang C. Charge-reversal nanoparticles: novel targeted drug delivery carriers. *Acta Pharm Sin B* 2016;**6**:261–7.
30. Ci LQ, Huang ZG, Liu Y, Liu ZP, Wei G, Lu WY. Amino-functionalized poloxamer 407 with both mucoadhesive and thermosensitive properties: preparation, characterization and application in a vaginal drug delivery system. *Acta Pharm Sin B* 2017;**9**:593–602.
31. Liu J, Li M, Luo Z, Dai L, Guo X, Cai K. Design of nanocarriers based on complex biological barriers *in vivo* for tumor therapy. *Nano Today* 2017;**15**:59–90.
32. Eetezadi S, Ekdawi SN, Allen C. The challenges facing block copolymer micelles for cancer therapy: *in vivo* barriers and clinical translation. *Adv Drug Deliv Rev* 2015;**91**:7–22.
33. Tan LW, Ma BY, Zhao Q, Zhang L, Chen LJ, Peng JR, et al. Toxicity evaluation and anti-tumor study of docetaxel loaded mPEG-Polyester micelles for breast cancer therapy. *J Biomed Nanotechnol* 2017;**13**:393–408.
34. Li Q, Liang J, You XR, Liu XJ, Wu HT, Gao W, et al. A novel reactive oxygen species triggered polymeric nanoplatform for controlled drug delivery and cancer therapy. *J Biomed Nanotechnol* 2017;**13**:513–21.
35. Wang YJ, Chen LJ, Tan LW, Zhao Q, Luo F, Wei YQ, et al. PEG-PCL based micelle hydrogels as oral docetaxel delivery systems for breast cancer therapy. *Biomaterials* 2014;**35**:6972–85.
36. Cai CL, Xie YX, Wu LL, Chen XJ, Liu HM, Zhou Y, et al. PLGA-based dual targeted nanoparticles enhance miRNA transfection efficiency in hepatic carcinoma. *Sci Rep* 2017;**7**:1–12.
37. Sun CT, Zhou L, Gou ML, Shi S, Tao L, Lang JY. Improved antitumor activity and reduced myocardial toxicity of doxorubicin encapsulated in MPEG-PCL nanoparticles. *Oncol Rep* 2016;**35**:3600–6.
38. Ma J, Shen M, Xu CS, Sun Y, Duan Y, Du LF. Biodegradable double-targeted PTX-mPEG-PLGA nanoparticles for ultrasound contrast enhanced imaging and antitumor therapy *in vitro*. *Oncotarget* 2016;**7**:80008–18.
39. Liang Y, Peng X, Chen Y, Deng X, Gao W, Cao J, et al. Chain length effect on drug delivery of chrysin modified mPEG–PCL micelles. *RSC Adv* 2015;**5**:59014–21.
40. Hao Y, Dong ML, Zhang TY, Peng JR, Jia YP, Cao YP, et al. Novel approach of using near-infrared responsive PEGylated gold nanorod

coated poly(L-lactide) microneedles to enhance the antitumor efficiency of docetaxel-loaded MPEG-PDLLA micelles for treating an A431 Tumor. *ACS Appl Mater Interfaces* 2017;**9**:15317–27.
41. Song W, Tang Z, Lei T, Wen X, Wang G, Zhang D, et al. The challenges facing block copolymer micelles for cancer therapy: *in vivo* barriers and clinical translation. *Adv Drug Deliv Rev* 2016;**12**:377–86.
42. Hu CY, Chen Z, Wu SJ, Han YF, Wang H, Sun HF, et al. Micelle or polymersome formation by PCL-PEG-PCL copolymers as drug delivery systems. *Chin Chem Lett* 2017;**28**:1905–9.
43. Liu GY, Zou JH, Tang QY, Yang XY, Zhang YW, Zhang Q, et al. Surface modified Ti_3C_2 MXene nanosheets for tumor targeting photothermal/photodynamic/chemo synergistic therapy. *ACS Appl Mater Interfaces* 2017;**9**:40077–86.
44. Li XJ, Munenobu T, Eiji Y, Atsushi H, Kon KJ. PEGylated PAMAM dendrimeredoxorubicin conjugate-hybridized gold nanorod for combined photothermal-chemotherapy. *Biomaterials* 2014;**35**:6576–84.
45. Kang SH, Kang KL, Huh H, Kim HJ, Chang SJ, Park TJ, et al. Reducing agent-assisted excessive galvanic replacement mediated seed-mediated synthesis of porous gold nanoplates and highly efficient gene-thermo cancer therapy. *ACS Appl Mater Interfaces* 2017;**9**:35268–78.
46. Deng Y, Li E, Cheng X, Zhu J, Lu S, Ge C, et al. Facile preparation of hybrid core–shell nanorods for photothermal and radiation combined therapy. *Nanoscale* 2016;**8**:3895–9.
47. Yang LP, He J, Wen Y, Yi WJ, Li QL, Lin LW, et al. Nanoscale photodynamic agents for colorectal cancer treatment: a review. *J Biomed Nanotechnol* 2016;**12**:1348–73.
48. Zhu KN, Zhu ZY, Zhou HO, Zhang JY, Liu SY. Precisely installing gold nanoparticles at the core/shell interface of micellar assemblies of triblock copolymers. *Chin Chem Lett* 2017;**28**:1276–84.
49. Cui HD, Hu DH, Zhang JN, Gao GH, Zheng CF, Gong P, et al. Theranostic gold cluster nanoassembly for simultaneous enhanced cancer imaging and photodynamic therapy. *Chin Chem Lett* 2017;**28**:1391–8.
50. Megan AM, Moustafa RKA, Lauren AA, Rachel DN, Mostafa AE. The most effective gold nanorod size for plasmonic photothermal therapy: theory and *in vitro* experiments. *J Phys Chem B* 2014;**118**:1319–26.
51. Liu XY, Wang XG, Liu T, Patrick K. Gold nanoparticles incorporated nematic gel micropillars capable of laser actuation at room temperature. *Macromolecules* 2016;**49**:8322–31.
52. Eun JH, Dae GC, Min SS. Targeted and effective photodynamic therapy for cancer using functionalized nanomaterials. *Acta Pharm Sin B* 2016;**6**:297–307.
53. Jia YP, Ma BY, Wei XW, Qian ZY. The *in vitro* and *in vivo* toxicity of gold nanoparticles. *Chin Chem Lett* 2017;**28**:691–702.
54. Kang JH, Ko YT. Lipid-coated gold nanocomposites for enhanced cancer therapy. *Int J Nanomedicine* 2015;**10**:33–45.
55. Wang XY, Zhang JS, Wang YT, Wang CP, Xiao JR, Zhang Q, et al. Multi-responsive photothermal-chemotherapy with drug-loaded melanin-like nanoparticles for synergetic tumor ablation. *Biomaterials* 2016;**81**:114–24.
56. Escudero FMA, Cepas V, Gonzalez MP, Badia LR, Diaz GME, Sainz RM, et al. Cellular uptake and tissue biodistribution of functionalized gold nanoparticles and nanoclusters. *J Biomed Nanotechnol* 2017;**13**:167–79.
57. Liu X, Zhang X, Zhu M, Lin GH, Liu J, Zhou ZF, et al. PEGylated Au@Pt nanodendrites as novel theranostic agents for computed tomography imaging and photothermal/radiation synergistic therapy. *ACS Appl Mater Interfaces* 2017;**9**:279–85.
58. Nathalie VD, Michael RH, Roland K. Improving efficacy of hyperthermia in oncology by exploiting biological mechanisms. *Int J Hyperthermia* 2016;**32**:446–54.
59. Cao ZY, Feng LZ, Zhang GB, Wang JX, Shen S, Li DD, et al. Semiconducting polymer-based nanoparticles with strong absorbance in NIR-II window for *in vivo* photothermal therapy and photoacoustic imaging. *Biomaterials* 2018;**155**:103–11.
60. Ren H, Liu JQ, Su FH, Ge SZ, Yuan AH, Dai WM, et al. Relighting photosensitizers by synergistic integration of albumin and peruorocarbon for enhanced photodynamic therapy. *ACS Appl Mater Interfaces* 2017;**9**:3463–73.
61. Liao JF, Li WT, Peng JR, Yang Q, Li H, Wei YQ, et al. Combined cancer photothermal-chemotherapy based on doxorubicin/gold nanorod-loaded polymersomes. *Theranostics* 2015;**5**:345–56.
62. Marco AN, Carlos WS, Lívia MS, Mateus RM, Maria DP, Alceu MS, et al. Interleukin-18 (IL-18) is equally expressed in inflammatory breast cancer and noninflammatory locally advanced breast cancer: a possible association with chemotherapy response. *Asia Pac J Clin Oncol* 2017:1–7.
63. Lena N, Tim H, Anders L, Lars H, Per E. The influence of hyperthermia on intracranial pressure, cerebral oximetry and cerebral metabolism in traumatic brain injury. *Ups J Med Sci* 2017;**122**:177–84.
64. Arlene LO, Lianne EMV, Caspar ML, Hans MR, Rosemarie C, Anneke MW, et al. Sensitizing thermochemotherapy with a PARP1-inhibitor. *Oncotarget* 2017;**8**:16303–12.
65. Heba E, Alaa R, Paras J, Mati UR, Li P, Zha QL, et al. Hyperthermia and radiation reduce the toxic side-effects of bufadienolides for cancer therapy. *Oncol Lett* 2017;**14**:1035–40.
66. Sharon SE, Elizabeth AR, Daniel TF. Fever and the thermal regulation of immunity: the immune system feels the heat. *Nat Rev Immunol* 2015;**15**:335–49.
67. Chang L, Liu XL, Fan DD, Miao YQ, Zhang H, Ma HP, et al. The efficiency of magnetic hyperthermia and *in vivo* histocompatibility for human-like collagen protein-coated magnetic nanoparticles. *Int J Nanomedicine* 2016;**11**:1175–85.
68. Tao Z, Cheng M, Wang SC, Lv W, Hu HQ, Li CF, et al. JAK2/STAT3 pathway mediating inflammatory responses in heatstroke-induced rats. *Int J Clin Exp Pathol* 2015;**8**:6732–9.
69. Cherryl Z, Jolien MB, Dharmindredew R, Jan DB. Hypothermia due to antipsychotic medication: a systematic review. *Front Psychiatr* 2017;**8**:165–73.
70. Heyke CD, Gereon H, Achim DG, Roy HP, Henning H. Localized thermal tumor destruction using dye-enhanced photothermal tumor therapy. *Lasers Surg Med* 2015;**47**:452–61.
71. Oh Y, Je JY, Madhappan SM, Seo H, Cho WH. pH and NIR-light-responsive magnetic iron oxide nanoparticles for mitochondria-mediated apoptotic cell death induced by chemo-photothermal therapy. *Int J Pharm* 2017;**531**:1–13.
72. Nikolaos MD, George T, Evangelos CB, Athanasia P, Melina M, Theodora M, et al. Gold nanoparticles, radiations and the immune system: current insights into the physical mechanisms and the biological interactions of this new alliance towards cancer therapy. *Pharmacol Ther* 2017;**178**:1–17.
73. Tan LW, Peng JR, Zhao Q, Zhang L, Tang XC, Chen LJ, et al. A novel MPEG-PDLLA-PLL copolymer for docetaxel delivery in breast cancer therapy. *Theranostics* 2017;**7**:2652–72.
74. Li WT, Peng JR, Tan LW, Wu J, Shi K, Qu Y, et al. Mild photothermal therapy/photodynamic therapy/chemotherapy of breast cancer by Lyp-1 modified docetaxel/IR820 co-loaded micelles. *Biomaterials* 2016;**106**:119–33.
75. João C, Nuria O, Zhang Y, Natalie A. Local triple-combination therapy results in tumour regression and prevents recurrence in a colon cancer model. *Nat Mater* 2016;**15**:1128–40.
76. Yang K, Feng LZ, Liu Z. Stimuli responsive drug delivery systems based on nano-graphene for cancer therapy. *Adv Drug Deliv Rev* 2016;**105**:228–41.
77. Yu J, Yin WY, Zheng XP, Tian G, Zhang X, Bao T, et al. Smart MoS_2/Fe_3O_4 nanotheranostic for magnetically targeted photothermal therapy guided by magnetic resonance/photoacoustic imaging. *Theranostics* 2015;**5**:931–45.
78. Yuan T, Anthony JM. Increasing the rate of heating: a potential therapeutic approach for achieving synergistic tumour killing in combined hyperthermia and chemotherapy. *Int J Hyperthermia* 2013;**29**:145–55.

79. Bert H, Peter W, Olaf A, Annette D, Geetha S, Thoralf K, et al. The cellular and molecular basis of hyperthermia. *Crit Rev Oncol Hematol* 2002;**43**:33–56.
80. Kawazoe H, Sumikawa S, Nakauchi K, Yakushijin Y, Yamamoto Y, Watanabe Y, et al. Preventive effect of pre-warming, hot compress, and pH adjustment in oxaliplatin-induced venous pain. *Int J Clin Pharm* 2017;**39**:1291–7.
81. Ni XF, Wu P, Wu J, Ji M, Tian B, Jiang ZX, et al. Hyperthermic intraperitoneal perfusion chemotherapy and response evaluation in patients with gastric cancer and malignant ascites. *Oncol Lett* 2017;**14**:1691–6.